Geophysical Journal International

Geophys. J. Int. (2016) **204,** 1662–1677 doi: 10.1093/gji/ggv558
GJI Seismology

Holocene surface ruptures of the Rurrand Fault, Germany—insights from palaeoseismology, remote sensing and shallow geophysics

Christoph Grützner,[1,*] Peter Fischer[2] and Klaus Reicherter[1]

[1]*Institute of Neotectonics and Natural Hazards, RWTH Aachen University, Lochnerstr.* 4–20, *D*-52064 *Aachen, Germany. E-mail: chg39@cam.ac.uk*
[2]*Institute for Geography, Johannes Gutenberg-Universität Mainz, Johann-Joachim-Becher-Weg* 21, *D*-55099 *Mainz, Germany*

Accepted 2015 December 30. Received 2015 December 1; in original form 2015 July 9

SUMMARY

The Lower Rhine Embayment in Central Europe hosts a rift system that has very low deformation rates. The faults in this area have slip rates of less than 0.1 mm yr^{-1}, which does not allow to investigate ongoing tectonic deformation with geodetic techniques, unless they cover very long time spans. Instrumental seismicity does only cover a small fraction of the very long earthquake recurrence intervals of several thousands of years. Palaeoseismological studies are needed to constrain slip rates and the earthquake history of such faults. Destructive earthquakes are rare in the study area, but did occur in historic times. In 1755/1756, a series of strong earthquakes caused significant destruction in the city of Düren (Germany) and the surrounding areas. In this study we document palaeoseismological data from the nearby Rurrand Fault. In contrast to earlier studies on the same fault, we found evidence for a surface rupturing earthquake in the Holocene, and we identified at least one more surface rupturing event. Our study shows that the Rurrand Fault currently accommodates deformation in earthquakes rather than by creeping. The coseismic offsets were determined to be between less than 0.5 m per event. We assign maximum possible magnitudes of M_w 5.9–6.8 for the Rurrand Fault and a slip rate of at least 0.02–0.03 mm yr^{-1} for the last ∼130–50 kyr. The surface ruptures did not occur at the main fault trace that has a clear morphological expression due to older tectonic motions, but on a younger fault strand in the hanging wall of the main fault. Terrain analyses based on 1 m resolution airborne LiDAR data have been used to image the subtle morphological expression of this young fault zone. Georadar and electric resistivity tomography were applied to image the fault zone at depth and to test if these shallow geophysical methods can be used to identify and trace the fault zone. Georadar failed to produce reliable results, but geoelectrics were successfully applied and allowed us to retrieve slip rate estimates. Our results indicate that the Düren 1755/1756 earthquakes did not produce surface ruptures at the Rurrand Fault, either because they did not rupture the surface at all, or because they occurred at another, neighbouring fault.

Key words: Geomorphology; Palaeoseismology; Seismicity and tectonics; Continental tectonics: extensional; Neotectonics; Europe.

1 INTRODUCTION

In slowly deforming regions faults have slip rates well below 1 mm yr^{-1} and earthquake recurrence intervals of thousands of years (Scholz 2002). Geodetic techniques are usually not capable of detecting such slow tectonic movements unless they cover several decades (e.g. Fuhrmann *et al*. 2014). The time period covered by instrumental seismicity is not sufficiently long to fully understand the faulting behaviour and to conclude on maximum magnitudes, fault segmentation and seismic hazard. Historical sources are often used to extend the observation time span (Gasperini *et al*. 1999) and palaeoseismological investigations aim on unravelling faulting history during the Holocene or even Pleistocene times (DuRoss *et al*. 2011). These techniques may provide valuable information, but usually come along with relatively

* Now at: COMET, Bullard Laboratories, Department of Earth Sciences, University of Cambridge, Madingley Rise, Madingley Road, CB3 0EZ Cambridge, United Kingdom.

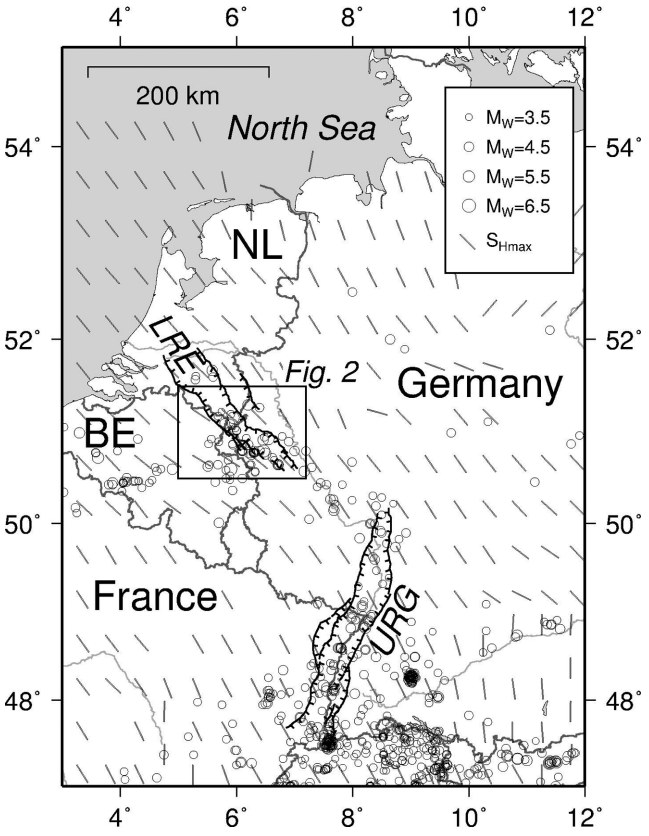

Figure 1. The Cenozoic European Rift System in northwest Europe. BE: Belgium; NL: the Netherlands; LRE: Lower Rhine Embayment; URG: Upper Rhine Graben. White dots represent the $>M_w$ 3.5 earthquakes of the European-Mediterranean Earthquake Catalogue for the last millennium (Grünthal & Wahlström 2012). Black bars mark the direction of the maximum horizontal stresses S_{Hmax} (data from Heidbach *et al*. 2010). The inset shows the extent of Fig. 2. This map is in Mercator projection.

large uncertainties. Historical sources can be biased, incomplete or of varying completeness, they may exaggerate or understate seismic shaking, they sometimes confuse seismic events with other phenomena or mix up cause and effect. The description of locations and earthquake effects is often vague or contradicting in different sources and historical documents might have been manipulated or modified afterwards. Still in many regions of the world, especially where long written records do exist, historical sources can significantly extend the knowledge on past seismicity (Albarello *et al*. 2001).

Palaeoseismological investigations are strongly depending on the location of the trench site. In slowly deforming regions geomorphological expressions of active faulting can be obscured by erosion and sedimentation and thus, make it difficult to choose proper trench sites. Structures related to surface faulting may vary strongly within short distances along fault strike and the reconstruction of a fault's rupture history is limited by the uncertainties in palaeoseismology that includes the accuracy of dating. Sedimentological features can sometimes be properly explained by different mechanisms (equifinality) and it is almost impossible to completely erase any subjectivity in the interpretation of palaeoseismological data.

These problems also arise in the Lower Rhine Embayment (LRE) in Western Germany. The area is an intraplate rift system (Fig. 1) with extensional tectonics and a set of normal faults in a horst and graben structure (Camelbeeck *et al*. 2007). Although the faults have very low slip rates of less than 0.1 mm yr^{-1}, the LRE bears among the highest seismic hazard in Germany and was subject of intense palaeoseismological investigations during the last decades (see summary in Vanneste *et al*. 2013). Historical records reach back hundreds of years and numerous historical events are known from written sources (Ahorner 1983; Hinzen & Reamer 2007). The strongest historical earthquake was the Düren earthquake of 1756 February 18 with a magnitude of M_w 5.8 (Grünthal & Wahlström 2003). No surface ruptures were reported and based on the available damage reports the event cannot clearly be ascribed to a certain fault. One possible candidate for the Düren earthquake(s) is the nearby Rurrand Fault. This fault has a suitable length for strong earthquakes, it is located close to the epicentral area, and its activity is evidenced by a geomorphological expression. Palaeoseismological studies have proven late Quaternary surface rupturing events, although there is some debate whether or not the trenches allow concluding on Holocene surface ruptures (Lehmann *et al*. 2001; Vanneste & Verbeeck 2001).

Here, we present new palaeoseismological and geophysical data from the Rurrand Fault to better understand its seismic behaviour and rupture history. Another aim of this study is to provide new data for identifying the fault causative for the Düren earthquakes.

2 GEOLOGICAL SETTING

In this section, we briefly describe the geological setting of the study area and its tectonic context. We then summarize the available data on instrumental and historical seismicity with a special emphasis on the 1755/1756 Düren seismic crisis. After that, we discuss previous palaeoseismological investigations in the study area, with a focus on the Rurrand Fault and possible Holocene surface ruptures.

2.1 Geological setting

The Lower Rhine Embayment comprises the southeastern part of the Lower Rhine Basin. It is bordered by the Rhenish Shield in the west, south and east, and opens to the North Sea in the northwest (Fig. 2). The LRE is part of the European Cenozoic Rift System (Fig. 1), which evolved mainly in the Neogene as a result of the lithospheric response to the Alpine Orogeny and the opening of the Atlantic (Ziegler 1992; Michon *et al*. 2003). The LRE is characterized by slow NE–SW extension and a set of normal faults that separate a number of NW-elongated tectonic blocks in a horst and graben style (e.g. Geluk *et al*. 1994; Houtgast & van Balen 2000). From NE to SW, the most important blocks are the Krefeld, Cologne, Venlo, Erft and Rur blocks (Fig. 2). The latter is also called the Roer Valley Graben, RVG. Most of the blocks are tilted towards the NE and show half-graben geometry, the subsidence rates vary.

The central Roer Valley Graben is the dominant structure and extends beyond the LRE to the NW (Roer is the Dutch name of what is the river Rur in Germany). This 20–30 km wide graben is the deepest in the LRE and its initiation dates back as far as to the Early Mesozoic (Geluk *et al*. 1994; van den Berg 1994). After being active in the Middle Jurassic and then again from Late Mesozoic onwards, the graben experienced several stages of inversion. During the Oligocene, subsidence prevailed; the still ongoing NE–SW extension of the RVG and the entire LRE started in the Oligocene–Miocene transition (Geluk *et al*. 1994; Michon *et al*. 2003; van Balen *et al*. 2005; Reicherter *et al*. 2008). Subsidence rates peaked in the Quaternary (Houtgast & van Balen 2000). The Cenozoic infill of the RVG reaches a thickness of about 1000 m at the NE boundary fault of the RVG. The other grabens experienced

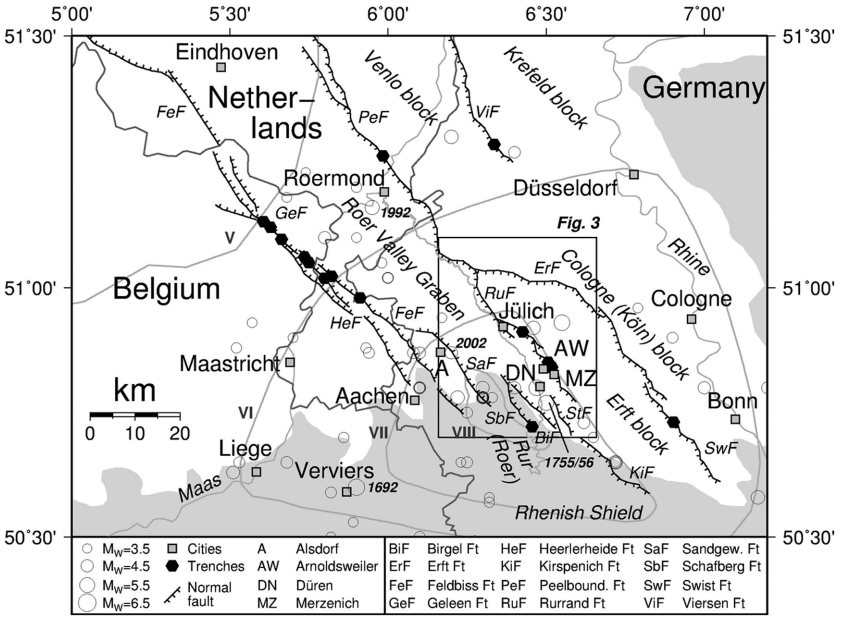

Figure 2. The Lower Rhine Embayment is characterized by a set of (sub-)parallel normal faults and dominated by the Roer Valley Graben. The Rurrand Fault has been trenched twice in the past—close to Jülich (Lehmann *et al*. 2001; Vanneste & Verbeeck 2001) and at the Merzenich site (Skupin *et al*. 2008). This paper presents new data from the Arnoldsweiler trench site. Light grey lines: rivers; Grey lines: macroseismic intensities of the 1756 February 18 Düren earthquake after Meidow (1995); Dark grey lines: national borders; Grey shaded area: Rhenish Shield; White dots: earthquakes from the Grünthal & Wahlström (2012) catalogue; Bold italic numbers: year and location of significant earthquakes. Inset shows location of Fig. 3. This map is in Mercator projection.

less subsidence, but the Neogene infill there is still in the order of some hundreds of meters (Schäfer *et al*. 2005). The Quaternary reaches thicknesses of more than 100 m in the RVG and up to 50 m elsewhere in the LRE. The Oligocene to recent infill of the grabens consists of several hundreds of meters of soft sediments.

In the German part of the LRE, a thick Oligocene layer of mainly marine sands is covered by the lignite-bearing Miocene, clayey-sandy units (Schäfer *et al*. 2005). The Messinian Hauptkies Fm and Kieseloolithes represent coarse sediments of a braided river system and serve as important stratigraphic markers. Pliocene formations are finer-grained braided river sands with occasional lacustrine clays and the youngest, but thin lignite layers in the LRE. The Plio-Pleistocene boundary is marked by the Reuver Clay, which is overlain by Pleistocene Rhine terraces. This terrace system has been extensively studied since it allows precise dating of the Quaternary evolution of the LRE (Boenigk & Frechen 2006). Cryoturbation occasionally affected the Pleistocene units and cryosols are known from Upper Weichselian units (Frechen *et al*. 2003; Boenigk & Frechen 2006). Similar sedimentary units are also present in other parts of the LRE (e.g. Schokker *et al*. 2005) and Houtgast *et al*. (2005) describe cryoturbation features found in a palaeoseismological trench at the Feldbiss Fault in detail. A Loess cover of few meters thickness is present in the entire study area.

2.3 Active tectonics

The faults that separate the tectonic blocks generally strike (W)NW–(E)SE and show pure dip-slip normal movement. This is consistent with the present-day overall European stress field, which is NW–SE directed (Reicherter *et al*. 2008; Heidbach *et al*. 2010; Fig. 1). Generally, the RVG is bounded by two major faults zones to the NE and to the SW. These faults are relatively straight and narrow features in the northwestern part of the graben, while in the southeast a greater number of segmented, parallel and subparallel faults constitute the graben's boundaries.

The NE dipping, southwestern boundary of the Roer Valley Graben in the LRE is formed by the Feldbiss Fault zone. This fault zone consists of a number of single major faults with some overlap. In Germany the Feldbiss Fault is the main structure, in the Netherlands the fault zone is comprised of the parallel Feldbiss, Geleen and Heerlerheide Faults. The Geleen Fault can be correlated to the Bree Fault in Belgium. At the SE tip of the Feldbiss Fault, the graben boundary steps to the NE in a set of almost parallel, partially overlapping faults, namely the Münstergewand, Sandgewand, Schafberg, Birgel and Stockheim Faults.

The entire SW boundary of the graben is ∼150 km long, with single fault segments reaching up to 40 km in length, although in some cases the segments do not necessarily mark a tectonic boundary (Vanneste *et al*. 2013). The NE boundary of the RVG has a similar length and is made up of the SW dipping Peelboundary Fault System in the NW. At the SE tip of this fault zone, the Erft-Swist Fault System continues, curving into E–W direction and then back to the NW–SE overall trend of the study area. Thus, the overall width of the RVG stays more or less the same along its strike. The Rurrand Fault, in contrast, continues linear in the same direction as the Peelboundary Fault for another ∼40 km, but joins the Peelboundary Fault trace in an ∼90° angle. Three single segments can be distinguished in the Rurrand Fault zone with slightly overlapping edges, but these are considered as one composite seismic source by Vanneste *et al*. (2013).

Fault dips in the LRE were determined by from palaeoseismological trenching, mining data, seismic profiles (e.g. Demyttenaere & Laga 1988; Dusar *et al*. 2001), and earthquake source parameters (Hinzen & Reamer 2007). The Rurrand Fault has a dip angle of 53–59° at depth, based on instrumental seismicity (Hinzen & Reamer 2007) and up to 75° based on trenching (Vanneste & Verbeeck 2001). Vanneste *et al*. (2013) conclude that most of the faults

in the LRE dip between 50° and 65° at depth. Close to the surface they often are steeper (e.g. Dusar *et al*. 2001) and can even appear to dip in the opposite direction in palaeoseismological trenches (e.g. Vanneste & Verbeeck 2001; Skupin *et al*. 2008).

Quaternary fault slip rates in the study area are very low and indicate slow intraplate deformation. The highest Quaternary slip rates of 0.07–0.09 mm yr^{-1} are observed at the longest structure in the LRE, the Peelboundary Fault (Vanneste *et al*. 2013). The Erft-Swist and Feldbiss Faults have slip rates between 0.05 and 0.07 mm yr^{-1}, respectively. For the Rurrand Fault, Vanneste & Verbeeck (2001) report a slip rate of 0.05–0.2 mm yr^{-1} based on palaeoseismological trenching for the last ∼40 kyr. Based on data from Ahorner (1962), Vanneste *et al*. (2013) estimate a slip rate for the Rurrand Fault between 0.03 and 0.05 mm yr^{-1} for the Quaternary. Most of the other faults in the study area move even slower (see review of fault slip rates in Vanneste *et al*. 2013). Slip rate estimates are generally based on offset stratigraphic markers and palaeoseismological investigations, as geodetic techniques currently lack the precision necessary to identify such low velocities, or they cover too short time intervals. Another problem with geodetic measurements in the LRE is the intense mining activity. The base of open pit lignite mines is as low as 370 m below surface (>250 m below sea level, Hambach mine) and the groundwater level is artificially lowered in the vicinity of the mines to allow for a dry floor. Ground subsidence since the 1960s ranges from a few centimetres up to a few meters in the study area, thus outpacing any tectonic movements (Campbell *et al*. 2002). Some authors concluded that aseismic creep would occur on most faults in the LRE (e.g. Ahorner 1996; Houtgast *et al*. 2003, 2005), but other studies cast doubts on this conclusion (see discussion in Camelbeeck *et al*. 2007).

2.3 Instrumental seismicity

The seismicity of the study area is among the highest in Central Europe (Fig. 1). The strongest instrumental earthquake was the Roermond (Netherlands) event of 1992 April 13, and had a magnitude of M_L 6.0 (Reamer & Hinzen 2004) or M_w 5.4 (Camelbeeck & van Eck 1994; Fig. 2). Only few other instrumental events exceeded M4 (Hinzen & Reamer 2007). Most of the seismicity is confined to the RVG boundary faults and indicates dip-slip movement. All earthquakes in the study area occur in less than 28 km depth (Reamer & Hinzen 2004). Most events cluster between 6–8 km and 14–18 km depth below surface based on the catalogue of the Royal Observatorium of Belgium (Vanneste *et al*. 2013).

2.4 Historical seismicity and the Düren earthquakes

The historical catalogues list several significant events since medieval times (Hinzen & Reamer 2007 and references therein; Leydecker 2011). Recent archeoseismological studies revealed damage patterns that could be caused by even older seismic events (Reicherter *et al*. 2011; Hinzen *et al*. 2012). None of the instrumental and historical events in the study area produced surface ruptures. This is likely due to their low magnitudes and to their rather large depths.

The strongest historical event in the Lower Rhine Embayment is the Düren earthquake of 1756. At the end of 1755, a series of seismic events initiated that lasted for more than 1 yr. Meidow (1995) reports more than 70 earthquakes that were felt in Düren and its vicinity. On 1756 February 18, a quake reached intensity VIII in the epicentral area between Düren and Eschweiler and was felt in up to 400 km distance (Sieberg 1940; Meidow 1995). Extensive building damage was caused by the event and at least one landslide was triggered. The earthquake probably had a magnitude of M_s 5.75 (Camelbeeck *et al*. 2007), M_L 6.1 (Meidow 1995) or M_w 5.8 (Grünthal & Wahlström 2003). Hinzen & Oemisch (2001) assign an intensity magnitude of M_{LI} 6.4. Neither primary nor secondary surface ruptures are known and thus the location of the causative fault is unclear. It is questionable if the Düren event ruptured the surface at all, because the assumed magnitude of M_w 5.8 does not necessarily imply this and is close to values that are often seen as a threshold for surface ruptures (*cf*. Michetti *et al*. 2005; McCalpin 2009). Given the uncertainties of historical data, it is not possible to link the earthquake to a certain fault merely based on the macroseismic observations.

2.5 Previous palaeoseismological investigations

Palaeoseismological investigations were carried out in the LRE in Belgium, in the Netherlands and in Germany during the last 20 yr. These studies aimed on extending the seismic catalogue, identifying the maximum possible magnitudes, revealing long-term slip rates, and estimating earthquake recurrence intervals. Trenching studies mainly concentrated on the main boundary faults of the RVG: In Belgium on the Bree Fault scarp (Camelbeeck & Meghraoui 1998; Vanneste *et al*. 1999; Meghraoui *et al*. 2000; Vanneste *et al*. 2001), in the Netherlands on the Feldbiss Fault, the Geleen Fault (Houtgast *et al*. 2003, 2005) and the Peelboundary Fault (van den Berg *et al*. 2002), and in Germany on the Viersen Fault, the Swist Fault, the Feldbiss Fault (Skupin *et al*. 2008), the Schafberg Fault (Kübler 2012) and the Rurrand Fault (Vanneste & Verbeeck 2001; Skupin *et al*. 2008). Additionally, the Viersen Fault (Skupin *et al*. 2008) was trenched (Fig. 2). The results of the trenching campaigns show that surface rupturing earthquakes occurred during the Late Quaternary. Based on coseismic offsets and mapped fault lengths, earthquakes with magnitude of up to ∼M_w 7.1 must be considered possible at the major fault zones. Due to the very low slip-rates, recurrence intervals for surface rupturing events are in the order of tens of thousands of years on each individual fault (Vanneste *et al*. 2013).

Most identified palaeoseismic events are pre-Holocene or cluster in a period around the end of the last glacial maximum, approx. 15 kyr, especially those on the southwestern boundary fault of the RVG (Houtgast *et al*. 2005). This led Houtgast *et al*. (2005) to speculate on a relation between glacial unloading and strong seismic events. There is evidence for a Holocene surface rupturing earthquake along the Bree Fault scarp (Vanneste *et al*. 2001), but this event was not identified in the neighbouring trenches on the same fault. Kübler (2012) reports two seismic events post-dating 7 kyr BP from the Schafberg Fault mainly based on secondary earthquake environmental effects, but no unambiguous Holocene surface ruptures were encountered in the trench.

The Rurrand Fault in Germany has been trenched close to the city of Jülich (Hinzen *et al*. 2001; Lehmann *et al*. 2001; Vanneste & Verbeeck 2001) and near Merzenich further to the southeast (Skupin *et al*. 2008). Vanneste & Verbeeck (2001) report a number of surface-rupturing palaeo-earthquakes from the Jülich trench site, including Holocene movements of 1.5–2.5 m based on OSL, U/Th and AMS radiocarbon dating. However, Lehmann *et al*. (2001) published a different interpretation of the same trench that excludes Holocene surface ruptures, but still suggests that surface rupturing earthquakes with several tens of centimetres of offset might have happened.

The Merzenich trench site revealed an offset of 0.8–1.0 m, which is likely linked to an event around 60–50 kyr (Skupin *et al*. 2008). No evidence for Holocene surface ruptures was encountered there. The Jülich trench is located relatively close to the centre of the fault, while the Merzenich site is only a few kilometres away from its southeastern tip, and the two locations belong to two different segments of the Rurrand Fault. Therefore, a surface rupturing event in Jülich not necessarily has been preserved as coseismic offset in the Merzenich trench. To conclude, Holocene surface ruptures in Germany, Belgium and the Netherlands remain highly debated.

3 STUDY SITE AND METHODS

Here we present detailed information on the study site and on the methods used. First, we describe the locality of our palaeoseismological investigations and its relative position at the fault. Then we briefly describe the methods that we used to obtain the palaeoseismological data. We carried out shallow geophysical prospection in order to image deeper parts of the fault and we aimed to investigate whether it would be possible to detect the fault zone prior to excavations or not. The geophysical methods and the data processing are documented in the last part of this chapter.

3.1 Study site

The Rurrand Fault is a ∼40 km long, NW–SE trending structure that dips towards the SW. The fault is segmented in three major strands (Vanneste *et al*. 2013). From north to south, these are the Linnich, Jülich and Düren sections (Fig. 3). They have lengths of 18, 12 and 16 km, respectively. The segments overlap at their tips for a few kilometres. There are hints that the three segments can rupture simultaneously in a major earthquake (Vanneste & Verbeeck 2001; Skupin *et al*. 2008), based on offsets observed in palaeoseismological trenches. The fault has a clear morphological expression along most of its strike (Hinzen *et al*. 2001), testifying to Quaternary activity. The palaeoseismological studies at the Jülich and Merzenich sites confirmed offset strata and fault structures where the topographical step is obvious.

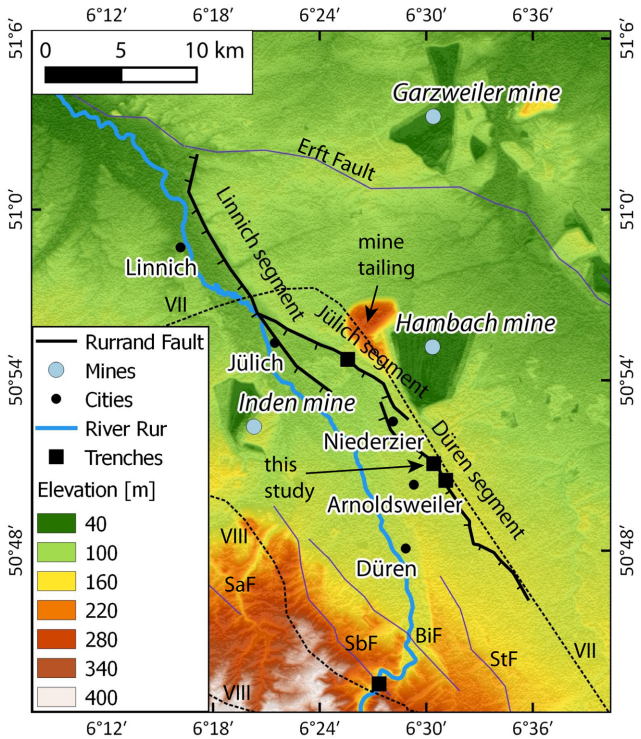

Figure 3. The three segments of the Rurrand Fault (thick black line, ticks on the hanging wall). Purple lines are other normal faults in the study area (see Fig. 2 for abbreviations). For the trenching results of the SbF see Kübler (2012). Dashed black line indicates isoseismals of the 1756 February 18 Düren earthquake from Meidow (1995). Topography is based on SRTM1 data. This map is in Mercator projection.

Our study site is located near Arnoldsweiler (N50°51′4″, E6°30′22″), less than 1.5 km away from the Merzenich trench, which is further to the SE along fault strike (Fig. 4). Arnoldsweiler marks one third of the Rurrand Fault away from its southwestern tip and is almost in the centre of the Düren section. A new part of the highway 4 from Aachen to Cologne was built during the last years, as the nearby open pit lignite mine Hambach was extended towards the south and reached the former course of the highway. In 2010, extensive earthworks were taken out at the study site, accompanied by archaeological investigations. At this occasion, the Düren section of the Rurrand Fault was exposed at several sites and accessible for a short period of time (Figs 4–6). We documented the available outcrops and extended them wherever possible. Most exposures are wide but shallow archaeological pits of less than 1 m depth, which allowed tracing the fault on the ground, thus already testifying to offset geological layers close to the surface and indicating relatively recent movement (Figs 6 and 7). The area was cropland for hundreds of years before the construction works started and has a well-developed, though not extensively thick plough zone. At one site, a 2 m high vertical outcrop cut the fault in an oblique angle and allowed to analyse deformation in great detail (trench 5609). A second excavation (trench 6064) exhibits the uppermost 1.5 m of the fault zone.

3.2 Trenching and OSL sampling

We enlarged the archaeological pits where this was possible and cleaned the trench walls in order to have a plain surface where all relevant units and the fault zone can clearly be identified. The outcrops were described in terms of colour (Munsell colour scheme), grain size, humidity and mineral content, and lithological units were identified based on these criteria. Earthquake-related deformation patterns were identified and documented. We sampled the uppermost (youngest) unit that has been deformed by the most recent surface-rupturing earthquake for OSL dating. The sample has been assigned the ID 5609 and the lab code C-L3216 and was sent to the Cologne Luminescence Lab at the Institute for Geography, University of Cologne. The polymineral fraction (4–11 μm), feldspar and quartz (100–200 μm) have been extracted for age determination. The single-aliquot regenerative-dose approach (SAR) was used for the measurements (*cf*. Murray & Wintle, 2000, 2003; Wallinga *et al*. 2000). The environmental dose rate was determined using high resolution gamma ray spectrometry. All details on the sample treatment are summarized in Table 1.

3.3 Geophysical investigations

We applied ground penetrating radar (GPR) for imaging the shallow subsurface. GPR emits electromagnetic energy into the ground and records amplitudes and travel times of reflected waves.

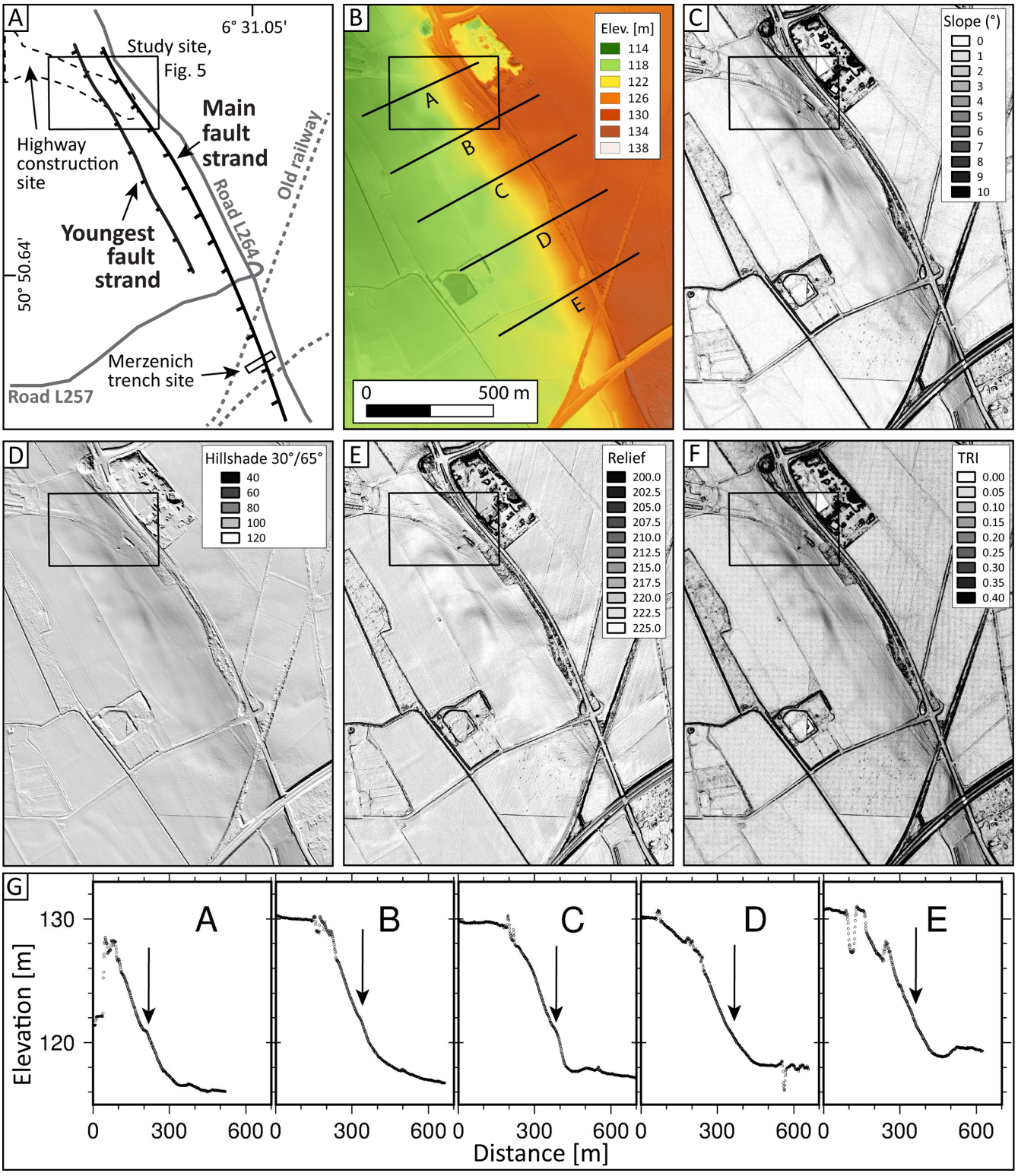

Figure 4. Morphological expression of the Rurrand Fault in the study area. The main fault was trenched at the Merzenich site (Skupin *et al*. 2008). The digital terrain model is based on 1 m airborne LiDAR data and copyright of Geobasis NRW 2012. (A) Sketch of the study area with the main morphological features and orientation points; (B) Elevation map, data range cut to 114–138 m a.s.l.; Letters A–F indicate the location of the profiles in panel G. (C) Slope angle, data range cut to 0–10°; (D) Hillshade map, light source is in the NNE (30°), illumination angle is 65°; (E) Relief map, data range cut to 200–225; (F) Terrain ruggedness index (TRI), data range cut to 0–0.4. (G) Topographic profiles across the fault scarp. Left is to the NE, right is to the SW. Arrows indicate the break in slope caused by the younger fault. Map projection is UTM with the GRS80 ellipsoid, datum ETR89 and elevation reference DHHN92.

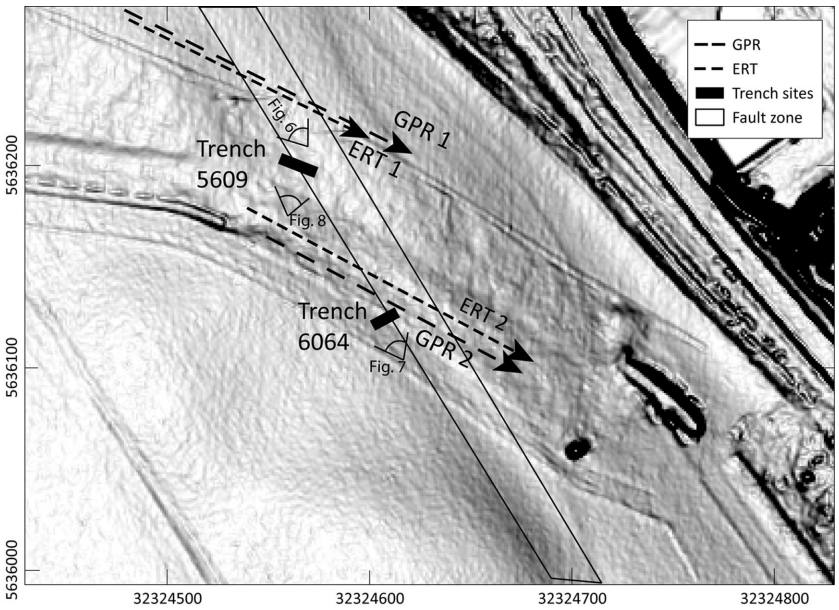

Figure 5. Detailed map of the study site. The fault zone is a few meters wide and its general trend outlined with the thin black lines. Two trenches were opened across the SW dipping Rurrand Fault, named after the nomenclature of the archaeological survey: Trench 5609 (Figs 8 and 9) and trench 6064 (Fig. 7). Triangular symbols indicate location and direction of photographs in the following figures. Dashed lines mark the location of the ground penetrating radar (GPR, Fig. 10) and electric resistivity tomography (ERT, Figs 11 and 12) surveys. Background is the slope angle calculated from airborne LiDAR data as in Fig. 4. The map extend is outlined in Fig. 4. Map projection is UTM with the GRS80 ellipsoid, datum ETR89 and elevation reference DHHN92.

Reflections occur where the electromagnetical parameters of the underground, especially the dielectric permittivity, abruptly change. Such changes can be due to layer boundaries, bedding planes, variations in the water content and other effects. A 270 MHz antenna was used combined with a survey wheel and a SIR-3000 controller (manufacturer: GSSI). This setup would probably allow more than 5 m of penetration under good conditions, in our case maximum achievable depth was ∼3 m. The resolution of the method mainly depends on the distance between the reflector and the antenna, the antenna frequency, and the dielectric permittivity of the ground. Here we achieved a maximum vertical resolution of ∼0.1 m close to the surface. Data processing was performed with ReflexW software of Sandmeier Scientific Software, Karlsruhe and included start time correction, background removal, and gain adjustments. A time-depth conversion was performed assuming a constant wave velocity of 0.14 m ns^{-1}, based on the results of a diffraction hyperbola analysis.

Electric resistivity tomography was applied in order to image the fault zone in greater depths. We used a Lippmann 4-point-light system with 80 electrodes and 1.5 m electrode spacing. Dipole–dipole, Schlumberger and Wenner geometry were used, respectively, along two parallel profiles. Data processing included the removal of bad datum points that were mainly caused by locally high contact resistances, and inversion using the Res2DINV software package. We also tested a capacity-coupled geoelectrics system, the Geometrics OhmMapper, but found much higher inversion errors, less resolution, and less penetration depth compared to the ERT system. This is very likely due to the rather high conductivities of the ground, which are unfavourable conditions for the use of this method.

The geophysical profiles were collected across the fault zone in an oblique angle, following the archaeological excavations. We recorded two GPR profiles and two ERT profiles (Fig. 5). For each ERT profile we measured dipole–dipole, Schlumberger and Wenner configuration.

4 RESULTS

In this section we document the morphological, palaeoseismological and geophysical expression of surface faulting at the Rurrand Fault. We first describe how the fault's morphology can be visualized with remote sensing data. The second part of this chapter focusses on the fault features that were found in the trenches, and we then present shallow geophysical data.

4.1 Fault morphology from LiDAR data

We used a digital elevation model (DEM) of the study area in order to investigate the morphological expression of the fault. The main fault strand is assumed to have developed the ∼15 m high gentle slope and its surface projection is probably located between the central and the upper part of the slope (Fig. 4A). The DEM is based on aerial LiDAR data with 1 m point spacing. We calculated slope angle, hillshade, relief and terrain ruggedness index and found that in the SW part of the main slope a thin linear feature can be identified in the data. This feature has a sharper expression than the main slope and runs parallel to the latter close to the slope's lower part (Figs 4B–F). The lineament marks a second strand of the Rurrand Fault, which crops out near the surface in the highway construction site. Towards the SE, the morphological expression vanishes and is finally lost close to the Merzenich trench site of Skupin *et al*. (2008, Fig. 4G). We consider this fault strand to have experienced more recent offset compared to the main fault, but less cumulative displacement.

4.2 Trenching results

Shallow pits of less than 1 m depth were dug for archaeological prospection at the highway construction site. The Rurrand Fault crops out in these excavations, indicating that even the youngest

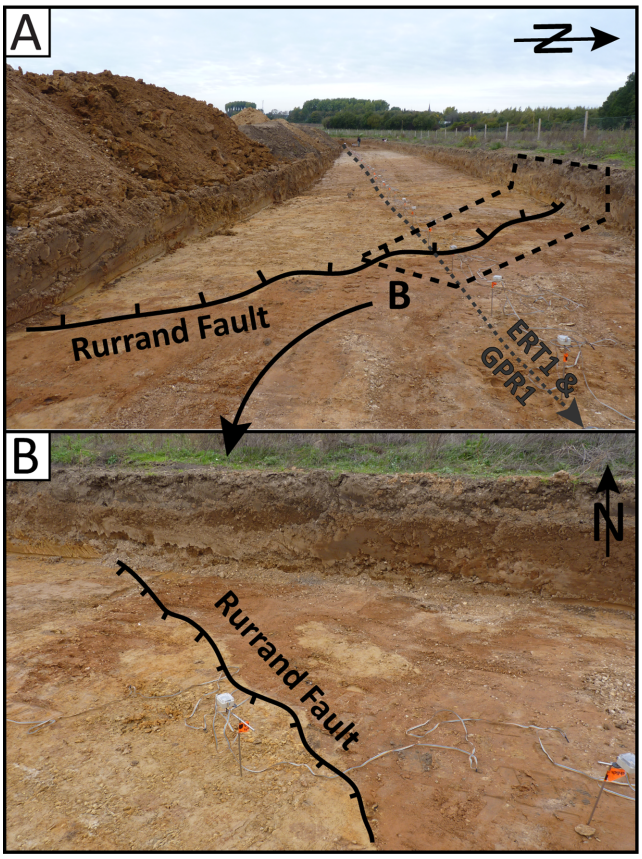

Figure 6. Fault outcrops in archaeological pits. (A) The Rurrand Fault is visible in the shallow archaeological excavations (<1 m depth) with an abrupt colour change at the surface. The grey dotted line marks the location of the shallow geophysical profiles ERT1 and GPR1. The position of the fault at the surface fits very well to the position of the geophysical anomalies. Dashed line marks the outline of Fig. 6(B); (B) Close up of the fault zone cropping out in silty-clayey and loess sediments. Note the electrodes of the geoelectrics device for scale.

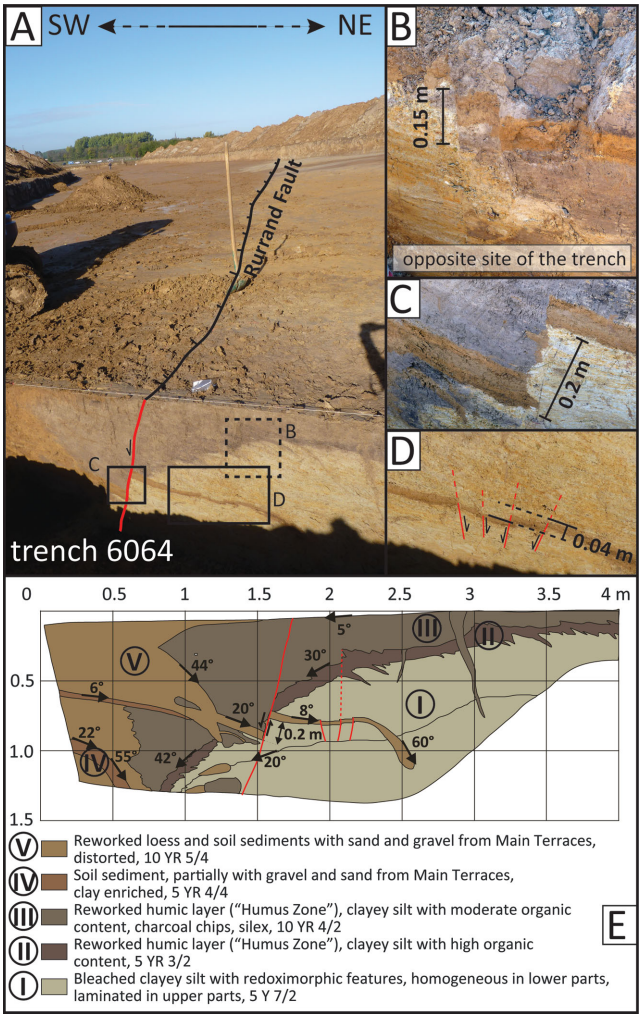

Figure 7. Trench 6064, exposing the Rurrand Fault and evidence for coseismic surface ruptures. (A) The trace of the fault is visible in the shallow archaeological excavations (<1 m depth) with an abrupt change in colour and it can be traced in the trench wall as a prominent crack. Solid black line: fault trace at the surface, ticks indicate fault dip; solid red line: fault trace in the trench wall; solid rectangles: location of close-ups of the trench wall shown in C and D; dashed rectangle: approximate location of inset B, which is located at the opposite trench wall 1.5 m towards the south; (B) Step-like offsets sum up to 0.15 m vertical displacement in the uppermost part of the outcrop, *ca*. 0.5 m northeast of the main fault trace; (C) 0.2 m of vertical offset is visible at the main fault trace with a ripped-off clast of the loessy, light-brown layer; (D) Minor vertical offsets in a graben style can be identified in the footwall; (E) Log of trench 6064, solid red lines indicate faults visible in the trench, the dashed red line indicates an inferred fault. The soil colours follow the Munsell colour scheme, arrows indicate apparent dip.

(Holocene) sediments ruptured coseismically (Figs 6A and B). Two larger pits (trenches 5609 and 6064) were analysed in detail for this study.

In general, we encountered Main Terrace (Lower-Middle Pleistocene) sands and gravels, overlain by Pleistocene interglacial and early glacial deposits. It is not clear if these units correspond to the Weichselian or to the Eemian, or represent even older interglacial stages. Above these units, (reworked) loess units, soil horizons and Holocene colluvium were present, which are likely Late Weichselian in age.

Trench 6064 is 1.5 m deep, 4 m wide and its top is ~0.8 m below present day surface. It cuts the Rurrand Fault almost perpendicularly. We assigned Roman numberals to the units that could be distinguished (Fig. 7). A fault zone that offsets loessic deposits is clearly visible in the center of the trench wall. It connects to the surface trace of the fault, which proves that it is not only a localized feature (Fig. 7A). This surface trace is marked by the contact of reworked loess and reworked humic sediments. The footwall is mainly made up of Pleistocene bleached clayey silt, in which a thin and deformed layer of reworked loess can be found. This layer partly contains gravels and sand from the Main Terrace. A thin, brownish reworked humic layer with a high organic content follows on top. The uppermost section of the foot wall is formed by a similar reworked humic layer, which has a lower organic content. These units are interpreted as Pleistocene, most likely interglacial or early glacial deposits such as pseudo-gleys, bleaching horizons and humic layers above Main Terrace sediments, which are not exposed here. The hanging wall does not contain the bleached clayey silt. Instead, its lowermost part is formed by loessic deposits with gravels and sands from the Main Terrace, interfingering with palaeosols and the reworked humic layer that also forms the top of the foot wall. Vertical offsets in these sediments are mainly restricted to the immediate fault zone (Figs 7B–D). In the uppermost part of the trench on its southern wall, 0.15 cm of vertical offset were encountered in a palaeosol (Fig. 7B), which is not preserved on the trench's

Table 1. Details on the sample treatment in the Cologne Luminescence Lab. Sample ID: 5609; Lab code: C-L3216; country: Germany; Lat/lon: 51 N, 6E; Altitude a.s.l.: 115 m; Depth: 0.5 m below surface; Year of Publication: 2013; Lum. Protocol: SAR-IRSL, SAR-OSL, Dose rate technique: Gamma Spec, Error level: 1 σ.

Mineral fraction	Lab. Code	Sample ID	Th (ppm)	*K* (per cent)	Depth (m)
Polymineral fraction	C-L3216	5609	2.54 ± 0.17	9.97 ± 0.71	1.64 ± 0.09
Feldspar	C-L3216	5609	2.54 ± 0.17	9.97 ± 0.71	1.64 ± 0.09
Quartz	C-L3216	5609	2.54 ± 0.17	9.97 ± 0.71	1.64 ± 0.09
Mineral fraction	Water content (per cent)	Mineral and grain size (mm)	Dose rate (Gy kyr^{-1})	De (Gy)	No. of subsamples
Polymineral fraction	20 ± 10	PM 4–11	3.50 ± 0.54	29.27 ± 1.47	20
Feldspar	20 ± 10	KF 100–200	3.19 ± 0.31	6.73 ± 0.93	34
Quartz	20 ± 10	Q 100–200	2.57 ± 0.30	6.71 ± 6.71	32
Mineral fraction	Age model	Age (kyr)	Fading corr. age (kyr)		
Polymineral fraction	CAM	8.36 ± 1.36	9.1 ± 1.5		
Feldspar	MAM	2.11 ± 0.36	2.3 ± 0.4		
Quartz	MAM	2.61 ± 0.48			

northern wall. A loessic layer is offset by 0.2 m at the main fault trace (Fig. 7C), and minor deformation can be found in the same layer further to the east (Fig. 7D). In total, ∼0.4 m of vertical offset is preserved in trench 6064 (Fig. 7E). The deformation features point to a rapid deformation instead of creep movement, and no gradual sedimentation was discovered in any unit.

Folding can be observed both in the hanging wall and in the footwall, where layers are bent towards the fault zone. In the case of the hanging wall the structure resembles a roll-over anticline, while the footwall can be seen as fault-related drag (Khalil & McClay 2002; Jin & Groshong 2006). We did not encounter similar structures in the other outcrops and their role in the accommodation of coseismic displacement remains unclear. For this reason we do not attempt to use these observations to derive fault parameters and to reconstruct the faulting/folding history, but concentrate our analysis on trench 5609 instead.

Trench 5609 cuts the Rurrand Fault in an oblique angle; it is 5 m wide and 2.5 m deep. This larger excavation enabled us to better understand the local stratigraphy and we assigned numbers to the units that could be identified (Fig. 8). The trench exhibits the fault zone that clearly offsets the lowermost units and almost reaches the surface. In the footwall, bleached Pleistocene units made up of clayey silts with redoximorphic features are found at the base (units 1, 3), which are likely interglacial or early glacial layers. Reworked humic layers with manganese mottles and a high organic content (unit 5) similar to those encountered in trench 6064 follow, covered by reworked loess (unit 6) that contains sand and gravel from the Main Terrace. The top is made up of a thick Holocene colluvial horizon (unit 7) and the recent plough zone (unit 8). The base of the hanging wall is formed by a clayey silt with sand and gravels (unit 2) that is overlain by bleached clayey silts of unit 3. A reworked humic layer with an intermediate organic content (unit 4) follows, overlain by units 5, 6, 7 and 8 as in the footwall. Two narrow vertical wedges filled with sand were encountered in the hanging wall, cutting units 4 and 5 (and probably 3) and being covered with unit 6. A SW-dipping crack with minor vertical, although not sharp, offset is visible in units 1 and 3 in the footwall, but does not reach unit 5. West of this feature a fault strand cuts all units from the base up to the top of unit 6, with a cumulative vertical offset of ∼0.5 m. In its upper part this SW-dipping fault branches into two distinct features. At the base of this fault, another fault zone branches to the SW, cutting units 1–5. This fault dips to the NW and ends in a crack filled with unit 7. Despite its shape this feature has

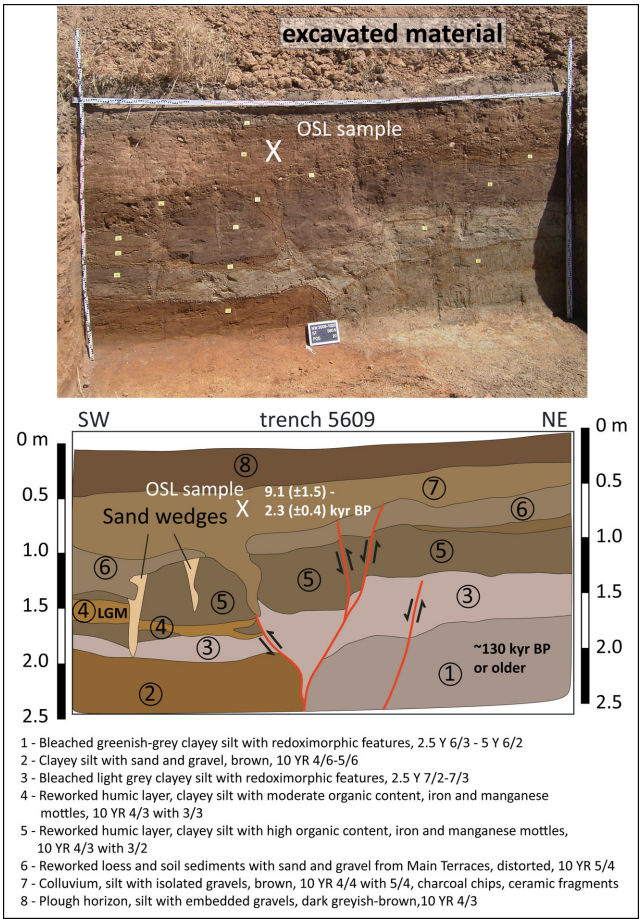

Figure 8. Trench 5609, exposing the Rurrand Fault (above) and sketch of the main fault features and sedimentary units (below). The X marks the location of the OSL sample which gave a minimum age of ∼2.3 kyr BP. The age of unit 4 is around Last Glacial Maximum (LGM). Unit 1 is ∼130 kyr or older.

no glacial origin, because it had formed when the Holocene unit 7 was already emplaced. Optical stimulated luminescence dating of unit 7 confirmed a Holocene age (maximum age: 9.1 ± 1.5 kyr BP; minimum age: 2.3 ± 0.4 kyr BP, see Table 1 for details). The plough zone is not affected by faulting.

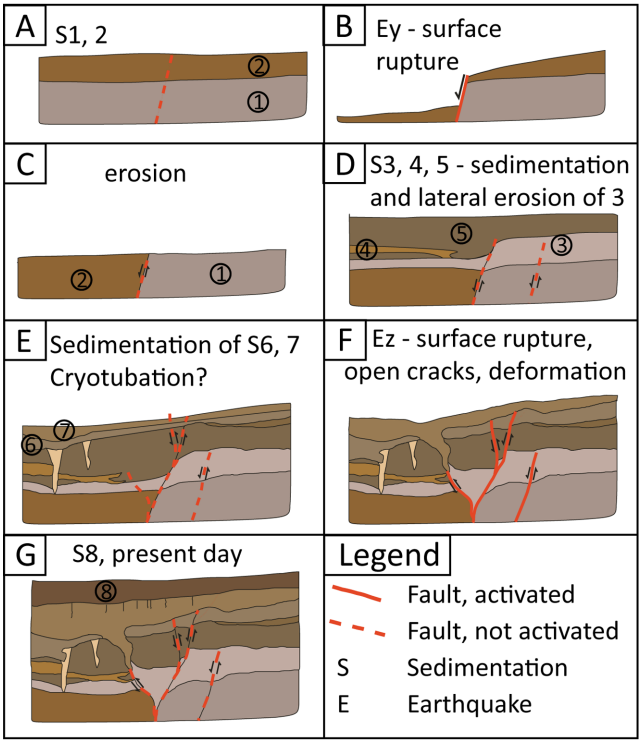

Figure 9. A possible reconstruction of the features observed in trench 5609, implying two surface-rupturing earthquakes. (A) Oldest phase—deposition of sedimentary units 1 and 2; (B) earthquake Ey creates a surface offset of probably ∼0.4 m; (C) erosion of unit 2 and planation of the surface; (D) deposition of units 3, 4 and 5. Lateral erosion of unit 3; (E) deposition of units 6 and 7, possibly formation of the sand wedges by cryoturbation (or another earthquake event?); (F) the most recent surface-rupturing earthquake causes open cracks which are filled with material from unit 7. A new fault strand is developed; (G) deposition of youngest sediments (unit 8) and development of recent soil, present day state.

4.3 Reconstruction of the observed deformation

We present a possible deformation history of trench 5609 in Fig. 9. Our interpretation includes two surface-rupturing earthquakes since the deposition of unit 1 (Figs 9B and F), followed by subsequent periods of quiescence and erosion/sedimentation, respectively. The narrow vertical wedges are interpreted to be glacial features (ice wedges), although a tectonic origin as open surface cracks is possible. The reconstruction demonstrates that surface-rupturing seismic events can explain the present-day state of the trench. The earliest event Ey likely led to an offset of more than 0.3 m at the surface. The most recent event Ez seems to have led to intense deformation and warping of the layers, and we estimate at least 0.3 m of vertical offset at the surface. More interestingly, the vertical wedge filled with unit 7 proves that this colluvium pre-dates the last event. We assume that liquefaction did occur during the last event, causing layer 6 to deform one of the ice wedges. OSL dating indicates a Holocene age for this event. We consider it possible that another surface rupturing event could have occurred in between Ey and Ez if the deformation of layer 4 had been caused seismically and not by cryoturbation.

4.4 Results of the geophysical survey

We applied shallow geophysical methods in order to image the fault at greater depths. GPR profile 1 did not provide any useful information, but the fault zone was detected in profile GPR 2. Fig. 10 presents a 70-m-long detail of the fault zone. The data cover ∼4 m depth and the fault trace was also visible at the surface.

The fault is marked by a sudden decrease in wave amplitudes, which points to an increase in electric conductivity and may be explained with higher water content in the fault zone. However, such zones do also occur elsewhere in the profile where no fault was present (e.g. at 122 m profile distance). The GPR data do in no way resemble the complex geometry that we encountered in the trenches. It is not possible to map the different units that were identified in the nearby trenches, and we cannot detect the multiple fault strands. There seems to be a general inclination of the sediments in the hanging wall towards the fault, but less so in the footwall. However, we consider it likely that an analyst without additional information from outcrops would have preferred a different interpretation. All the units that we encountered in the trenches are characterized by a relatively high electric conductivity, which results in a strong attenuation of the electromagnetic waves emitted by the radar system. Despite these unfavourable conditions, the penetration depth surprisingly appears to reach 3–4 m in some areas of the profile (e.g. between 130 and 140 m profile distance). We assume that the units in the shallow subsurface simply have very similar electromagnetic properties, especially dielectric permittivity and electric conductivity, and can therefore not be distinguished with GPR.

The ERT profile 1 reveals a subsurface structure that can be described by two layers (Fig. 11). A thin low resistivity layer of ∼3 m thickness in the NW and 2 m thickness in the SE is present at the surface (30–80 Ωm), followed by a layer with relatively higher resistivities between 200 and 400 Ωm. The base of the latter exceeds the depth of the ERT profile (25 m). We interpret the upper layer as the clayey-silty units encountered in the trenches and the lower layer as sands and gravels of the Main Terrace. The terrace appears two have two zones with especially high resistivity values, which could be due to internal variation of grain size. The step in the thickness of the upper layer is located where the fault crops out at the surface, and we therefore interpret this as 1 m vertical downthrow at the fault zone. The fault zone is more clearly visible in profile ERT2 (Fig. 12). As in the previous profile, a layer of 3 m thickness and resistivity values lower than 80 Ωm is present at the surface. In the NW part of the profile similar and occasionally slightly higher values are encountered below this layer to at least 25 m depth, while the SE part is characterized by values between 200 and 400 Ωm, as in ERT1. The latter is likely to represent a sand-gravel layer, while the lower resistivities are typical for clayey-silty sediments. The fault zone crops out at the surface where the remarkable change in the electric properties is observed in the ERT data, and we consequently interpret the resistivity change as indicative for a downthrown hanging wall. The minimum amount of downthrow can be derived from the data. The fact that we do not see the top of the Main Terrace units in the NW part suggests at least 25 m of vertical throw since the formation of the Main Terrace in the (Lower) Pleistocene at this strand of the Rurrand Fault.

5 DISCUSSION

5.1 Fault migration

The results of our study show that a Holocene surface rupturing earthquake occurred at the Rurrand Fault between 9.1 (±1.5) and 2.3 (±0.4) kyr BP, and at least one older event at the same site.

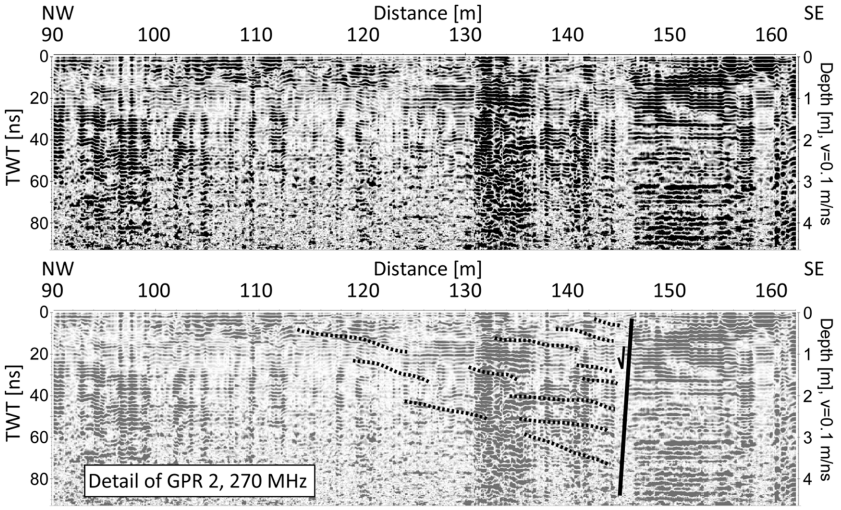

Figure 10. Ground penetrating radar profile GPR2, see Fig. 5 for location. The upper image shows the data, the lower one the interpretation. Dashed lines mark possibly dipping strata, the solid black line indicates the fault. Dipping layers can be observed in the hanging wall only, and only the uppermost parallel layers are not affected by rotation.

This is in contrast to the findings of Skupin *et al*. (2008), who trenched the Rurrand Fault only a few hundred meters SE of our study area and assigned an age of ∼50–60 kyr for the youngest surface rupturing event. These authors report a possible vertical offset of 1 m in a single event, while our study suggest that offsets of less than 0.5 m did occur in the last two events, respectively. It can be excluded that the observed deformation is due to creep or ongoing subsidence due to groundwater extraction, because of the formation of open surface cracks that were filled with Holocene sediments, the lack of prograding sedimentary features related to slow and quasi-steady deformation, and because of the brittle-like deformation style, which implies high strain rates. We argue the Rurrand Fault has developed a parallel fault strand parallel to its main fault trace, on which the most recent seismic movements did occur and might continue to occur in the future. Therefore, its morphologic expression is only minor at present, although we show that it can be detected with high resolution LiDAR data and geophysical methods.

We cannot rule out that the two strands of the Rurrand Fault join north of the Merzenich trench site, but the rather old deformation there implies that they do not rupture simultaneously.

5.2 Variability of ruptures

An interesting observation is the large variety of deformation features. Total offsets varied significantly between neighbouring trenches and outcrops (Figs 7 and 8), and also the deformation pattern itself is highly heterogeneous (e.g. Figs 7B–D and 9B, F). ERT data imply 1 m offset of the top of the Main Terrace in profile 1, but more than 25 m offset in profile 2. These observations illustrate the difficulties of palaeoseismological investigations on slow active faults and similar geological settings. Assumptions on fault slip rates and maximum magnitudes can be highly depending on the local conditions at the trench site. Our data suggest that future palaeoseismological studies on similar normal faults need to take these problems into account, and that geophysical and remote sensing reconnaissance for trench site selection should be extended in hanging wall direction.

5.3 Last surface rupturing earthquake

Vanneste & Verbeeck (2001) report Holocene surface ruptures on the central segment of the Rurrand Fault from a trench near Jülich, despite Lehmann *et al*. (2001) do not support this interpretation and claim much older, pre-Holocene events. According to Vanneste & Verbeeck (2001), the most recent seismic event is assigned an age of possibly AD 400–1670 if solifluction occurred or at least between 400 BC and AD 640 if this is not the case. The authors interpret their findings as indicative for 1.5–2.5 m vertical offset. While an age of <400 BC would fit our data, we did not find the same amount of displacement, but rather surface offsets one magnitude lower. We find it impossible to relate the two events based on the available data and we note that it remains unclear if the Rurrand Fault ruptured more than one segment during the last event that we found. If the fault ruptured all three segments, then a normal slip distribution (with the maximum slip in the centre of the fault) could explain the differences in offset, as the Jülich trench is located almost in the fault's centre (Fig. 2). However, the amount of slip that is visible at the surface is known to be variable along fault strike, especially in complex ruptures (e.g. Fletcher *et al*. 2014), and conclusions on palaeoearthquake magnitude based on point observations may be flawed. We must consider that the slip did not or not entirely reach the surface at some places, governed by local lithology and fault geometry, and also that surface offsets are not or only partially preserved in the geological record.

5.4 Maximum earthquake magnitudes

Based on fault lengths and widths published by Vanneste *et al*. (2013) and assuming a rigidity of $\mu = 3 \times 10^{10}$ N m^{-2}, we can estimate the potential seismic moment release for the Rurrand Fault and calculate moment magnitudes (Hanks & Kanamori 1979). In the following we assume a maximum seismogenic thickness of 25 km because of the recent seismicity pattern (Reamer & Hinzen 2004), and a fault width not exceeding the rupture length.

A slip of 0.5 m at the 16 km long Düren segment would correspond to M_w 6.4. If the two southern segments of the Rurrand Fault ruptured together (the 12 km Jülich segment and the 16 km

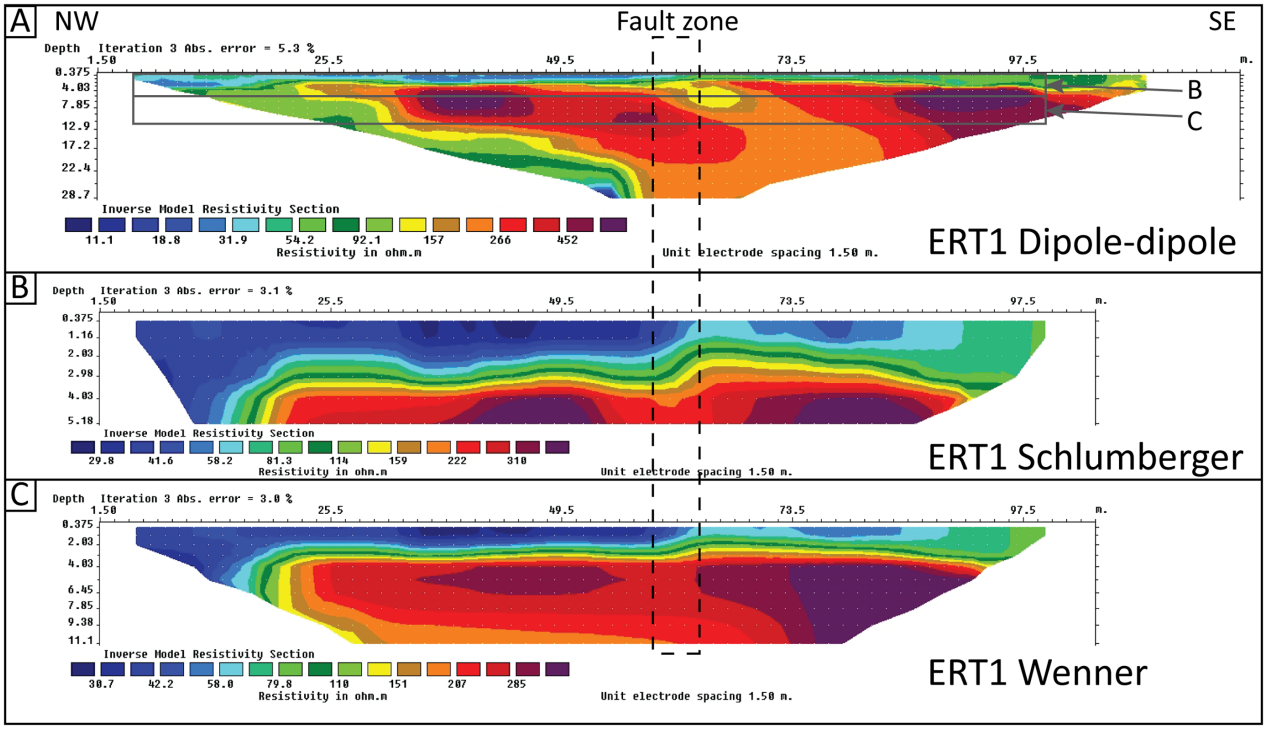

Figure 11. Electric tomography resistivity profile ERT1, see Fig. 5 for location. (A) Dipole–dipole configuration; (B) Schlumberger configuration; (C) Wenner configuration. Note that Schlumberger and Wenner cover shallower depths only as indicated with the grey lines in (a). A low resistivity layer of 2–3 m thickness is present at the surface, followed by a significant increase in resistivity with depth. The fault zone (see Fig. 6) is characterized by a small step in the resistivity distribution only, with the western side of the fault being apparently downthrown. Due to the limited length of the profile it remains unclear whether the end of the high resistivity layer at the beginning of the profile is related to another fault zone.

Düren segment), M_w 6.7 would be possible with 0.5 m slip and M_w 6.8 could be reached if all three segments failed (39 km length due to overlapping segments). These numbers are somewhat lower than those proposed by Vanneste *et al*. (2013), but an earthquake of this size would very likely have a huge impact today. We note that we might underestimate the amount of slip based on trench logs and that we cannot exclude that the main strand of the fault also moved coseismically during the events that we identified in the trenches.

The empirical relationships of Wells & Coppersmith (1994) result in slightly different values. A rupture length of 16 km (Düren segment) would imply a magnitude of *M*6.4, a rupture of all three segments and 39 km lengths would give *M*7.0 (for normal faults). A displacement of 0.5 m corresponds to magnitudes between *M*6.4 (max. displacement) and *M*6.6 (average displacement).

5.5 Slip rate

We observed not more than 1 m of surface offsets in units that are probably Weichselian or Eemian in age (~130–50 kyr), but may be older. This would correspond to a vertical displacement rate of not more than 0.02 mm yr^{-1} since that time. This value is close to the minimum value commonly assumed (see review in Vanneste *et al*. 2013), but probably much lower. The more than 25 m offset at the top of the Lower-Middle Pleistocene Main Terrace revealed by ERT data results in a long-term slip rate of at least 0.03 mm yr^{-1}. There are several possible explanations for this misfit: (1) our trenches do not expose the entire amount of surface faulting; (2) Our reconstruction could underestimate the amount of slip that occurred at the trench site; (3) the fault strand is younger than we assume and has had earthquakes in a shorter time period only; (4) some significant slip occurred at the main fault strand as well; (5) We overestimate the age of the offset layers, which we consider unlikely as the sediments are clearly indicative of interglacial conditions, and overlain by well dated Holocene layers and (6) the fault moves much slower than expected, which would in turn mean that all other palaeoseismic and geologic constraints on the slip rates are wrong, which we also consider unlikely. To conclude, we assume that our observations mark a minimum slip rate only. The value fits reasonably well with modelling results (Kaiser *et al*. 2005) and other observations (Vanneste *et al*. 2013).

5.6 Earthquake recurrence interval

In our trenches we identified two events since probably 50–130 kyr, which results in a recurrence interval of 25–65 kyr for surface rupturing events. If the slip rate of 0.02 mm yr^{-1} is correct, then 25 kyr would be sufficient to build up enough stress to be released in an event with 0.5 m of slip. This is in agreement with the interpretations of Vanneste & Verbeeck (2001) from the Jülich trench site (Table 2). A slip rate of 0.04 mm yr^{-1} would indicate that 1 m of deformation would build up within the lower bounds of the recurrence interval. Similar to the slip rate issue discussed above, we must take into account the uncertainties related to trench interpretation, retrodeformation, and surface offset distribution. Additional events that ruptured not the young fault strand but the main fault instead would lead to shorter recurrence intervals. We emphasize that the recurrence interval of surface rupturing earthquakes at the Rurrand Fault must be equal or longer than the recurrence interval of significant earthquakes here in general, because not all events do necessarily break the surface.

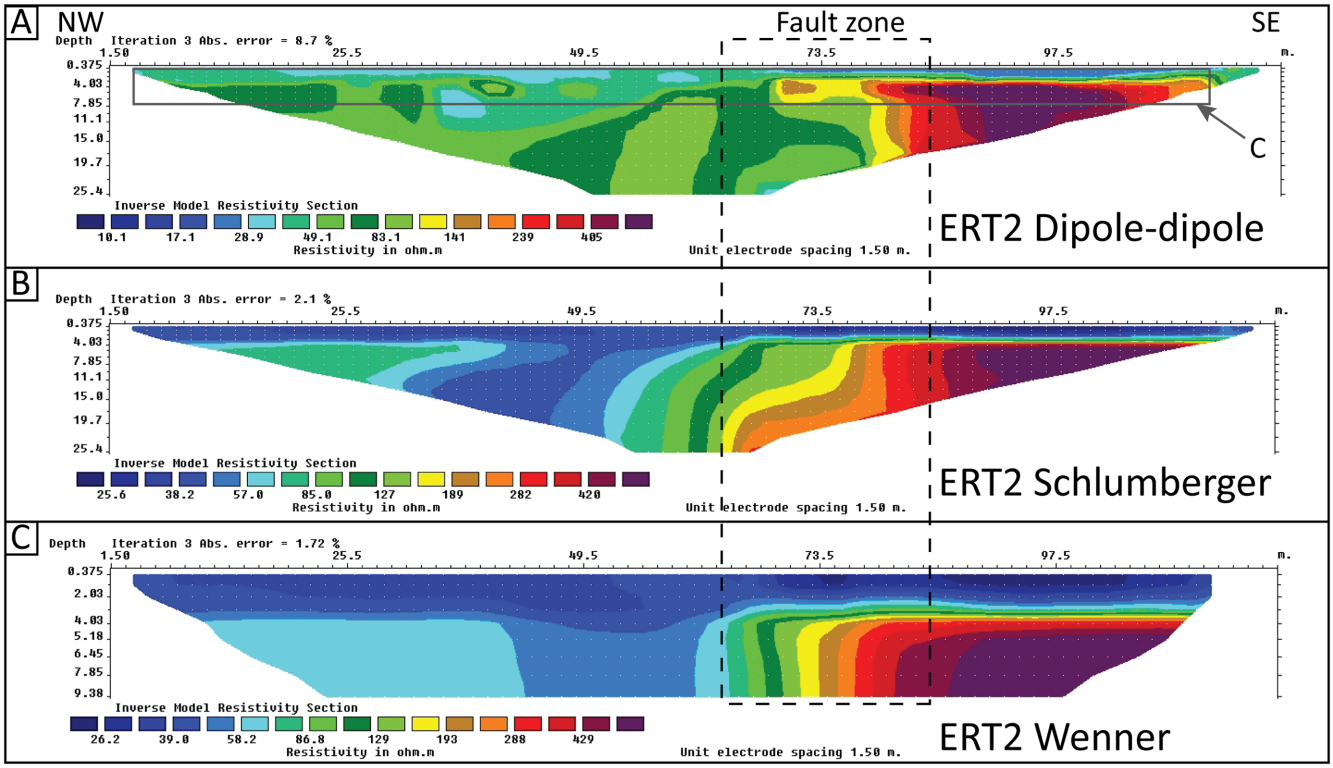

Figure 12. Electric tomography resistivity profile ERT2, see Fig. 5 for location. (A) Dipole–dipole configuration; (B) Schlumberger configuration; (C) Wenner configuration. Note that Wenner covers a shallower depth only as indicated with the grey lines in A. The low resistivity layer of 2–3 m thickness found in ERT1 is here present too, followed by a significant increase in resistivity with depth. The fault zone is clearly visible and characterized by the end of the high resistivity layer at around 65–75 m profile distance. The resistivity contrast might be due to different lithologies on both sides of the fault, but as well be influenced by variations in the water content.

Table 2. Simplified summary of the palaeoseismological investigations at the Rurrand Fault. Note that for the Jülich trench we only list the interpretation of Vanneste & Verbeeck (2001), not the ones of Lehmann *et al*. (2001) who do not interpret coseismic motion.

Trench site	Merzenich (Skupin *et al*. 2008)	Jülich (Vanneste & Verbeeck 2001)	Arnoldsweiler (this study)
Fault segment	Düren	Jülich	Düren
Surface rupturing events	(I) 50–60 kyr BP	(III) between 1.5–0.3 kyr BP and present (II) between 2.3 and 1.4 kyr BP (IIb) between 2.3–1.4 kyr BP and 43.4 ± 12.6 kyr BP?] (I) between [10-]117 and 130–185 kyr BP	(II) between 2.3 (±0.4) and 9.1 (±1.5) kyr BP (I) post-130 kyr BP
Offset per event	(I) 0.8–1.0 m	(III) >1 m (II) >1.5–2.5 m (IIb) >1.4–2.4 m?] (I) >1 m	(II) ≤0.5 m (I) ≤0.5 m
Recurrence interval	–	29–62 kyr	25–60 kyr
Slip rate	–	0.05–0.20 mm yr^{-1}	>0.02–0.03 mm yr^{-1}

5.7 A possible relation with isostatic rebound and deglaciation

Houtgast *et al*. (2005) speculate on a relation between glacial unloading and strong seismic events at the end of the last glacial maximum, as palaeoearthquakes seem to cluster around 15 kyr BP. Brandes & Winsemann (2013) and Brandes *et al*. (2015) also report that the last glaciation induced seismicity in northern Central Europe. Hoffmann & Reicherter (2012) report Late Pleistocene seismites from NE Germany. It is well known that the elastic rebound after deglaciation lead to a dramatic increase in seismicity for example in Scandinavia, a region which is still uplifting but nowadays characterized by low to intermediate earthquake activity (e.g. Mörner 1985; Fjeldskaar *et al*. 2000; Mörner, 2004, 2005; Olesen *et al*. 2004). The same observation was made in Eastern Canada (e.g. Adams 1989). Given the very long recurrence intervals of surface rupturing earthquakes in the LRE, it will naturally be hard to approach this issue with statistical observations. Our results imply that surface-rupturing events can occur well after peak deglaciation on locked faults.

The seismic hazard posed by this kind of faults is illustrated by the effects of the Düren earthquakes in 1755/1756 and more recent smaller events in the LRE. With the new data presented here we have to consider that larger, surface rupturing events did happen in the very recent geological past as well.

5.8 The Rurrand Fault and the Düren 1755/56 earthquake series

Our most recent event caused at least 0.3 m of vertical surface offset between 9.1 (±1.5) and 2.3 (±0.4) kyr BP. No younger surface rupture was observed. We assume that this event represents the starting point for a new earthquake cycle, which on average lasts more than 25 kyr for surface rupturing events. If the last event happened close to the lower time limit, enough stress could have built up to allow another earthquake to happen in 1755/1756. If the last event occurred rather late in the Holocene, this is more unlikely. In any case did the Düren earthquake series not produce surface ruptures at the Rurrand Fault. These earthquakes might have happened on another nearby fault, for example, the Stockheim Fault, or they did not rupture the surface, which is not unusual given their magnitude of M_s 5.75 (Camelbeeck *et al*. 2007) or M_L 6.1 (Meidow 1995). Several faults meet the three criteria that make them potential candidates for the Düren earthquake of 1756 February 18: (1) being long enough to produce a magnitude 6–6.5 earthquake; (2) being located close enough to the epicentral area and (3) being active. Among them are the Stockheim Fault, the Schafberg (Merode) Fault, the Sandgewand Fault, and the Rurrand Fault. Of these faults, the composite Rurrand Fault is the longest seismic source and the one with clearest morphological expression.

6 CONCLUSIONS

Our palaeoseismological investigations enhance the knowledge about the Rurrand Fault in the Lower Rhine Embayment and help to reconstruct the earthquake history in this intraplate setting with its slow active faults. We have presented data that indicate a Holocene surface rupturing earthquake in the Lower Rhine Embayment. Our observations show that surface displacements of 0.1–0.5 m occurred repeatedly at the Arnoldsweiler site. Recurrence intervals for these events appear to exceed 25 kyr, and a slip rate between 0.02 and 0.04 mm yr^{-1} is likely. We are able to show that the Rurrand Fault did not rupture the surface during the Düren 1755/1756 seismic crisis and conclude that these events likely occurred on another nearby fault system or did not rupture the surface at all. We demonstrate that earlier palaeoseismological investigations on this fault failed to recognize the most recent ruptures because the most recent movements did not occur at the main fault trace, but on a smaller parallel fault strand towards the hanging wall. We present high-resolution LiDAR data that allow recognizing this fault in the study area. Geophysical investigations (GPR and ERT) were used to image the fault zone. Georadar did not produce reliable results, which we ascribe to the high clay content of the subsurface and the loess. Electric resistivity tomography has proven to be a useful tool for imaging the fault zone and allowed estimating a long-term slip rate. Our data imply that strong seismic events of up to M_w 6.8 must be considered possible at the Rurrand Fault although they appear to have very large recurrence intervals. The palaeoseismic events that we found do not clearly correlate with periods in the past when post-glacial rebound was at its maximum, but the small number of known palaeoearthquakes make a statistical evaluation of a possible correlation difficult. In addition to the hazard posed by seismic shaking, the surface displacement hazard must be considered for the Rurrand and similar faults.

This study exemplifies that the on-fault deformation pattern is likely to be very heterogeneous in this geological setting, a lesson that should not be neglected in further palaeoseismological investigations in this area. Our data demonstrate that during the most recent tectonic period, the Rurrand Fault ruptured seismically and did not release stress by aseismic creep. Although the LRE is characterized by slow active faults with slip rates not exceeding 0.1 mm yr^{-1}, large earthquakes are possible. Each single fault has a very long earthquake recurrence interval, but the relatively large number of capable faults in the area makes clear that regional intense shaking will occur much more often. Owing to the very low slip rates, geodetic investigations like GPS currently fail to properly measure tectonic movements in the LRE. InSAR data are able to reveal localized subsidence related to groundwater extraction (Caro Cuenca *et al*. 2013) but cannot reveal tectonic movements here, because of the lack of coherence and the very slow deformation along the faults. Current seismicity in the LRE is among the highest in Central Europe, but the observation period remains short compared to the average recurrence interval of seismic events. We suggest that a combination of high-resolution surface data (e.g. airborne LiDAR), shallow geophysics and palaeoseismological trenching is currently the only way to understand the tectonics in such slow deforming regions.

ACKNOWLEDGEMENTS

The authors thank Jonas Winandy for his help in the field and Daniela Hülle for OSL dating. Thanks are extended to Klaus Lehmann, Simon Kübler and Tom Rockwell for fruitful discussions in the field. Thomas Ibeling conducted most of the archaeological work. CG wishes to express his gratitude to Andy Howell. Christian Brandes, Ronald van Balen, an anonymous reviewer, and the editor provided very valuable comments and suggestions which helped to improve the manuscript. The LiDAR data were kindly provided by the Geodatenzentrum North Rhine-Westphalia (Geobasisdaten der Kommunen und des Landes NRW © Geobasis NRW 2012). Some figures were created with the Generic Mapping Tools software package (Wessel & Smith 1998).

REFERENCES

Adams, J., 1989. Postglacial faulting in eastern Canada: nature, origin and seismic hazard implications, *Tectonophysics,* **163**(3), 323–331.

Ahorner, L., 1962. Untersuchungen zur quartären Bruchtektonik der Niederrheinischen Bucht, *Eiszeitalter und Gegenwart,* **13**, 24–105.

Ahorner, L., 1983. Historical seismicity and present-day microearthquake activity of the Rhenish Massif, Central Europe, in *Plateau Uplift,* pp. 198–221, eds Fuchs, K., von Gehlen, K., Mälzer, H., Murawski, H. & Semmel, A., Springer-Verlag.

Ahorner, L., 1996. How reliable are speculations about large paleoearthquakes at the western border fault of the Roer valley graben near Bree, in *Comptes-Rendus des 81ièmes: Journées Luxembourgeoises de Géodynamique,* pp. 39–57, ed. Bonatz, M., Grand Duchy of Luxemburg.

Albarello, D., Camassi, R. & Rebez, A., 2001. Detection of space and time heterogeneity in the completeness of a seismic catalog by a statistical approach: an application to the Italian area, *Bull. seism. Soc. Am.,* **91**(6), 1694–1703.

Boenigk, W. & Frechen, M., 2006. The Pliocene and Quaternary fluvial archives of the Rhine system, *Quarter. Sci. Rev.,* **25**(5), 550–574.

Brandes, C. & Winsemann, J., 2013. Soft-sediment deformation structures in NW Germany caused by Late Pleistocene seismicity, *Int. J. Earth Sci.,* **102**(8), 2255–2274.

Brandes, C., Steffen, H., Steffen, R. & Wu, P., 2015. Intraplate seismicity in northern Central Europe is induced by the last glaciation, *Geology,* doi:10.1130/G36710.1.

Camelbeeck, T. & Meghraoui, M., 1998. Geological and geophysical evidence for large paleo-earthquakes with surface faulting in the Roer Graben (northwest Europe), *Geophys. J. Int.,* **132,** 347–362.

Camelbeeck, T. & van Eck, T., 1994. The Roer Valley Graben earthquake of 13 April 1992 and its seismotectonic setting, *Terra Nova,* **6**(3), 291–300.

Camelbeeck, T. *et al.*, 2007. Relevance of active faulting and seismicity studies to assessments of long-term earthquake activity and maximum magnitude in Intraplate Northwest Europe, between the lower Rhine Embayment and the North Sea, *Geol. Soc. Am., Spec. Paper,* **425,** 193–224.

Campbell, J., Kumpel, H.J., Fabian, M., Fischer, D., Gorres, B., Keysers, C.J. & Lehmann, K., 2002. Recent movement pattern of the Lower Rhine Embayment from tilt, gravity and GPS data, *Neth. J. Geosci.,* **81**(2), 223–230.

Caro Cuenca, M., Hooper, A.J. & Hanssen, R.F., 2013. Surface deformation induced by water influx in the abandoned coal mines in Limburg, The Netherlands observed by satellite radar interferometry, *J. appl. Geophys.,* **88,** 1–11.

Demyttenaere, R. & Laga, P., 1988. Breuken- en isohypsenkaarten van het Belgisch gedeelte van de Roerdal Slenk: Eerste resultaten van een seismisch onderzoek in het gebied van Poppel-Lommel-Maaseik, *Professional Paper Belgische Geologische Dienst,* 1988/4.

DuRoss, C.B., Personius, S.F., Crone, A.J., Olig, S.S. & Lund, W.R., 2011. Integration of paleoseismic data from multiple sites to develop an objective earthquake chronology: application to the Weber segment of the Wasatch fault zone, Utah, *Bull. seism. Soc. Am.,* **101**(6), 2765–2781.

Dusar, M., Rijpens, J., Sintubin, M. & Wouters, L., 2001. Plio-Pleistocene fault pattern of the Feldbiss fault system (southern border of the Roer Valley Graben, Belgium) based on high resolution seismic data, *Geologie en Mijnbouw,* **80,** 79–93.

Fjeldskaar, W., Lindholm, C., Dehls, J.F. & Fjeldskaar, I., 2000. Postglacial uplift, neotectonics and seismicity in Fennoscandia, *Quarter. Sci. Rev.,* **19**(14), 1413–1422.

Fletcher, J.M. *et al.*, 2014. Assembly of a large earthquake from a complex fault system: surface rupture kinematics of the 4 April 2010 El Mayor–Cucapah (Mexico) Mw 7.2 earthquake, *Geosphere,* **10**(4), 797–827.

Frechen, M., Oches, E.A. & Kohfeld, K.E., 2003. Loess in Europe—mass accumulation rates during the Last Glacial Period, *Quarter. Sci. Rev.,* **22**(18), 1835–1857.

Fuhrmann, T., Westerhaus, M., Zippelt, K. & Heck, B., 2014. Vertical displacement rates in the Upper Rhine Graben area derived from precise leveling, *J. Geod.,* **88**(8), 773–787.

Gasperini, P., Bernardini, F., Valensise, G. & Boschi, E., 1999. Defining seismogenic sources from historical earthquake felt reports, *Bull. seism. Soc. Am.,* **89**(1), 94–110.

Geluk, M.C., Duin, E.J.Th., Dusar, M., Rijkers, R.H.B., Van den Berg, M.W. & Van Rooijen, P., 1994. Stratigraphy and tectonics of the Roer Valley Graben, *Geologie en Mijnbouw,* **73,** 129–141.

Grünthal, G. & Wahlström, R., 2003. An Mw based earthquake catalogue for central, northern and northwestern Europe using a hierarchy of magnitude conversions, *J. Seismol.,* **7**(4), 507–531.

Grünthal, G. & Wahlström, R., 2012. The European-Mediterranean earthquake catalogue (EMEC) for the last millennium, *J. Seismol.,* **16**(3), 535–570.

Hanks, T.C. & Kanamori, H., 1979. A moment magnitude scale, *J. geophys. Res.,* **84,** 2348–2350.

Heidbach, O., Tingay, M., Barth, A., Reinecker, J., Kurfeß, D. & Müller, B., 2010. Global crustal stress pattern based on the World Stress Map database release 2008, *Tectonophysics,* **482,** 3–15.

Hinzen, K.G. & Oemisch, M., 2001. Location and magnitude from seismic intensity data of recent and historic earthquakes in the northern Rhine area, Central Europe, *Bull. seism. Soc. Am.,* **91**(1), 40–56.

Hinzen, K.G. & Reamer, S.K., 2007. Seismicity, seismotectonics, and seismic hazard in the Northern Rhine area, in *Continental Intraplate Earthquakes: Science, Hazard, and Policy Issues,* pp. 225–242, eds Stein, S. & Mazzotti, S., Geological Society of America.

Hinzen, K.G., Reamer, K. & Rose, T., 2001. Results of Analysis of Digital Elevation Models Used Site Selection for Paleoseismological Investigations at the Rurrand Fault, *Geologie en Mijnbouw,* **80,** 109–117.

Hinzen, K.G., Schreiber, S., Fleischer, C., Reamer, S.K. & Wiosna, I., 2012. Archeoseismic study of damage in Roman and Medieval structures in the center of Cologne, Germany, *J. Seismol.,* **17**(2), 399–424.

Hoffmann, G. & Reicherter, K., 2012. Soft-sediment deformation of Late Pleistocene sediments along the southwestern coast of the Baltic Sea (NE Germany), *Int. J. Earth Sci.,* **101**(1), 351–363.

Houtgast, R.F. & van Balen, R.T., 2000. Neotectonics of the Roer Valley Rift System, the Netherlands, *Global Planet. Change,* **27,** 131–146.

Houtgast, R.F., van Balen, R.T., Kasse, C. & Vandenberghe, J., 2003. Late Quaternary tectonic evolution and aseismic near surface fault displacements along the Geleen Fault (Feldbiss Fault Zone - Roer Valley Rift System, the Netherlands), based on trenching, *Neth. J. Geosci./Geologie en Mijnbouw,* **82**(2), 177–196.

Houtgast, R.F., van Balen, R.T. & Kasse, C., 2005. Late Quaternary evolution of the Feldbiss Fault (Roer Valley Rift System, the Netherlands) based on trenching, and its potential relation to glacial unloading, *Quarter. Sci. Rev.,* **24**(3), 489–508.

Jin, G. & Groshong, R.H., 2006. Trishear kinematic modeling of extensional fault-propagation folding, *J. Struct. Geol.,* **28**(1), 170–183.

Kaiser, A., Reicherter, K., Hübscher, C. & Gajewski, D., 2005. Variation of the present-day stress field within the North German Basin—insights from thin shell FE modeling based on residual GPS velocities, *Tectonophysics,* **397**(1), 55–72.

Khalil, S.M. & McClay, K.R., 2002. Extensional fault-related folding, northwestern Red Sea, Egypt, *J. Struct. Geol.,* **24**(4), 743–762.

Kübler, S., 2012. Active tectonics of the Lower Rhine Graben (NW Central Europe): based on new paleoseismological constraints and implications for coseismic rupture processes in unconsolidated gravels, *Doctoral dissertation,* Universitätsbibliothek der Ludwig-Maximilians-Universität.

Lehmann, K., Klostermann, J. & Pelzing, R., 2001. Paleoseismological investigations at the Rurrand Fault, Lower Rhine Embayment, *Geologie en Mijnbouw,* **80**(3/4), 139–154.

Leydecker, G., 2011. Erdbebenkatalog für Deutschland mit Randgebieten für die Jahre 800 bis 2008, *Geologisches Jahrbuch,* **E 59,** 1–198.

McCalpin, J.P., 2009. *Paleoseismology,* 2nd edn, Academic Press, 613 pp.

Meghraoui, M., Camelbeeck, T., Vanneste, K., Brondeel, M. & Jongmans, D., 2000. Active faulting and paleoseismology along the Bree fault, lower Rhine graben, Belgium, *J. geophys. Res.,* **105**(B6), 13 809–13 841.

Meidow, H., 1995. Rekonstruktion und Reinterpretation von historischen Erdbeben in den nördlichen Rheinlanden unter Berücksichtigung der Erfahrungen bei dem Erdbeben von Roermond am 13. April 1992, *Dissertation,* Universität Köln, Leverkusen, 305 pp.

Michetti, A.M., Audemard, F.A. & Marco, S., 2005. Future trends in paleoseismology: integrated study of the seismic landscape as a vital tool in seismic hazard analyses, *Tectonophysics,* **408,** 3–21.

Michon, L., van Balen, R.T., Merle, O. & Pagnier, H., 2003. The Cenozoic evolution of the Roer Valley Rift System integrated at a European scale, *Tectonophysics,* **367**(1), 101–126.

Mörner, N.A., 1985. Paleoseismicity and geodynamics in Sweden, *Tectonophysics,* **117**(1), 139–153.

Mörner, N.A., 2004. Active faults and paleoseismicity in Fennoscandia, especially Sweden. Primary structures and secondary effects, *Tectonophysics,* **380**(3), 139–157.

Mörner, N.A., 2005. An interpretation and catalogue of paleoseismicity in Sweden, *Tectonophysics,* **408**(1), 265–307.

Murray, A.S. & Wintle, A.G., 2000. Luminescence dating of quartz using an improved single-aliquot regenerative-dose protocol, *Rad. Meas.,* **32,** 57–73.

Murray, A.S. & Wintle, A.G., 2003. The single aliquot regenerative dose protocol: potential for improvements in reliability, *Rad. Meas.,* **37,** 377–381.

Olesen, O. *et al.*, 2004. Neotectonic deformation in Norway and its implications: a review, *Norwegian J. Geol.,* **84**(1), 3–34.

Reamer, S.K. & Hinzen, K.G., 2004. An earthquake catalog for the Northern Rhine Area, Central Europe (1975–2002), *Seismol. Res. Lett.,* **75**(6), 713–725.

Reicherter, K. *et al.*, 2008. Alpine Tectonics II – Central Europe north of the Alps, in *The Geology of Central Europe: Mesozoic and Cenozoic,* pp. 1233–1286, ed. McCann, T., Geological Society of London.

Reicherter, K., Schaub, A., Fernández-Steeger, T., Grützner, C. & Kohlberger-Schaub, T., 2011. Aquisgrani terrae motus factus est (part 2): evidence for medieval earthquake damage in the Aachen Cathedral (Germany), *Quatern. Int.,* **242**(1), 149–157.

Schäfer, A., Utescher, T., Klett, M. & Valdivia-Manchego, M., 2005. The Cenozoic Lower Rhine Basin–rifting, sedimentation, and cyclic stratigraphy, *Int. J. Earth Sci.,* **94**(4), 621–639.

Schokker, J., Cleveringa, P., Murray, A.S., Wallinga, J. & Westerhoff, W.E., 2005. An OSL dated middle and late quaternary sedimentary record in the Roer Valley Graben (southeastern Netherlands), *Quarter. Sci. Rev.,* **24**(20), 2243–2264.

Scholz, C.H., 2002. *The Mechanics of Earthquakes and Faulting,* Cambridge Univ. Press.

Sieberg, A., 1940. Beiträge zum Erdbebenkatalog Deutschlands und angrenzender Gebiete für die Jahre 58 bis 1799*,* Mitteilungen des Deutschen Reichs-Erdbebendienstes, Reichsverlagsamt Berlin.

Skupin, K. *et al.*, 2008. Arbeitsergebnisse aus dem Geologischen Dienst Nordrhein-Westfalen*,* Krefeld, Scriptum 17.

van Balen, R.T., Houtgast, R.F. & Cloetingh, S.A.P.L., 2005. Neotectonics of the Netherlands, *Quarter. Sci. Rev.,* **24,** 439–454.

Van den Berg, M., Vanneste, K., Dost, B., Lokhorst, A., Van Eijk, M. & Verbeeck, K., 2002. Paleoseismic investigations along the Peel Boundary Fault: geological setting, site selection and trenching results, *Neth. J. Geosci.,* **81**(1), 39–60.

Van den Berg, M.W., 1994. Neotectonics of the Roer Valley rift system. Style and rate of crustal deformation inferred from syn-tectonic sedimentation, *Geologie en Mijnbouw,* **73,** 143–156.

Vanneste, K. & Verbeeck, K., 2001. Paleoseismological analysis of the Rurrand Fault near Jülich, Roer Valley graben, Germany: coseismic or aseismic faulting history?, *Geologie en Mijnbouw,* **80**(3-4), 155–169.

Vanneste, K., Meghraoui, M. & Camelbeeck, T., 1999. Late Quaternary earthquake-related soft-sediment deformation along the Belgian portion of the Feldbiss Fault, Lower Rhine Graben system, *Tectonophysics,* **309**(1), 57–79.

Vanneste, K., Verbeeck, K., Camelbeeck, T., Paulissen, E., Meghraoui, M., Renardy, F., Jongmans, D. & Frechen, M., 2001. Surface-rupturing history of the Bree fault scarp, Roer Valley graben: evidence for six events since the late Pleistocene, *J. Seismol.,* **5**(3), 329–359.

Vanneste, K., Camelbeeck, T. & Verbeeck, K., 2013. A model of composite seismic sources for the Lower Rhine Graben, Northwest Europe, *Bull. seism. Soc. Am.,* **103**(2A), 984–1007.

Wallinga, J., Murray, A.S. & Wintle, A.G., 2000. The single-aliquot regenerative dose (SAR) protocol applied to coarse-grain feldspar, *Rad. Meas.,* **32,** 529–533.

Wells, D.L. & Coppersmith, K.J., 1994. New empirical relationships among magnitude, rupture length, rupture width, rupture area, and surface displacement, *Bull. seism. Soc. Am.,* **84**(4), 974–1002.

Wessel, P. & Smith, W.H.F., 1998. New, improved version of the Generic Mapping Tools released, *EOS, Trans. Am. geophys. Un.,* **79,** 579.

Ziegler, P.A., 1992. European Cenozoic rift system, *Tectonophysics,* **208**(1), 91–111.